Energy Proceedings
Vol 26, 2022
ISSN 2004-2965

Understanding the Effect of Ion Concentration on Interfacial Resistance in Carbon Nanotube Membrane via Molecular Dynamics Simulation[#]

Yiru Su [1], Lang Liu [1*]
Key Laboratory of Low-Grade Energy Utilization Technologies and Systems, Ministry of Education, School of Energy and Power Engineering, Chongqing University, Chongqing 400044, China

ABSTRACT

The influence of ions concentration and CNT diameter on the interfacial resistance for CNT membrane is revealed through molecular dynamics approach. We find that the interfacial resistance of CNT membrane is affected by ion concentration and CNT diameter, and the reduction diameter can promote the interfacial resistance with the increase of ion concentration. The presence of ions in the system results in the increase of entrance-exit resistance and flange resistance composing the interfacial resistance.

Keywords: interfacial resistance, CNT membrane, ion concentration, CNT diameter

1. INTRODUCTION

Membrane technology due to its superiority and obvious advantages has attracted extensive attention as a promising solution to the separation challenge [1, 2]. The membrane acts as a selective barrier, allowing selective penetration of certain chemical or biological species[3, 4]. Membranes are currently widely used in water purification [5], air filtration [6], lithium separation [7, 8] and energy storage [9]. According to the size, the membrane can be divided into microfiltration membrane, ultrafiltration membrane and nanofiltration membrane. In the nanofiltration membrane, due to significant mechanical, thermal, electrical and chemical properties, the carbon nanotubes have been as an ideal material [10-14]. Corry studied the separation efficiency of salt solution through CNT membrane under hydrostatic pressure by MD simulation [15]. Yang et al. studied the separation process of Mg^{2+} and Li^{+} with CNT membrane [16].

In view of the application potential of nanofiltration membranes, it is very important to fully understand the flow mechanisms in nanofiltration membranes. Interfacial resistance is the one of the important factors which attracts many researchers' attention. Suk et al. studied the process of water molecules flowing into CNT membrane with non-equilibrium molecular dynamics simulation [17]. They found that there was an energy barrier at the interface of CNT membrane and the value is larger than the internal energy barrier by an order of magnitude. Liu et al. obtained the interfacial resistance of CNT membrane through diffusion coefficient of molecular diffusion rate and proved that the interfacial resistance was the main factor hindering the flow [18]. By studying the flow of water in CNT membranes, Zhang et al. found that the interfacial resistance was caused by the hydrogen bond rearrangement of water molecules at the interface [19]. In our previous work, we found that the interface resistance could be decomposed into the entrance-exit resistance and flange resistance [20]. However, few people have studied the effect of ions on the interface resistance, and the membrane to separate the ion is widely used in industry, such as the separation of Mg^{2+} and Li^{+} ions from salt lakes.

Against this backdrop, the present study aims to investigate the influence of ions on interfacial resistance from a microscopic perspective to overcome the gap in the existing literature. The LiCl/$MgCl_2$ solution was selected to be studied. In the sections that follow, we first analyzed the influence of ion concentration on the interface resistance, and then the reasons revealed by analyzing the entrance-exit resistance and flange resistance.

2. SIMULATION MEATHOD

2.1 Simulation Detail

In order to study the influence of ions in $MgCl_2$/LiCl mixed solution on the interfacial resistance, a simulation system is constructed as shown in Figure 1. The simulation system is set as a CNT membrane positioned at the center of the system box, connecting two bulk reservoirs with ions solution. The CNT membrane is made up of CNT with two graphene sheets located at the mouths of CNT. The diameter of CNT studied in this work ranges from 1.085 nm to 2.340 nm, corresponding to the (8,8) CNT and (15,15) CNT, respectively. The thickness of all CNT membranes investigated in this work is fixed at

10.0 nm. The membrane surface area is set to be identical for all cases during the simulation process with the cross-sectional area of reservoir ($L_x \times L_y$) as $3.68 \times 3.80\ \mathrm{nm}^2$. In order to study the effect of ion concentration on transport, three different concentrations are selected, 0.5 M, 1.0 M and 1.5 M, with the ion concentration ratio (c_{MgCl_2}/c_{LiCl}) fixed at 1:1.

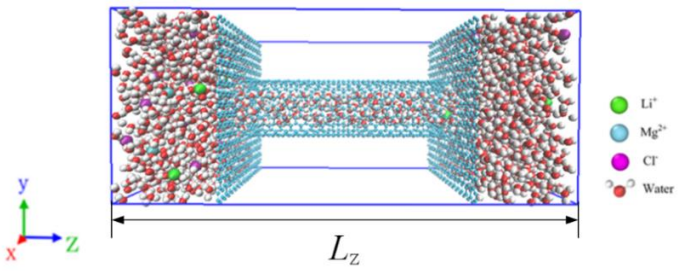

Fig. 1. Illustration of the simulation system for a 10.0 nm thick (10, 10) CNT with 0.5 M

The SPC/E model is applied to describe the interactions between water molecules and the interactions between CNT and other atoms/ions are described by 12-6 Lennard-Jones potential. The detailed parameters for the potentials come from the ref [21, 22]. Periodic boundary conditions are applied in all three dimensions. To obtain the flux of water molecules through the CNT membrane, the nonequilibrium molecular dynamics (NEMD) simulations are performed by applying a driving force to the ionic solution in CNT. A 10.0 MPa driving pressure is applied to make the whole system flow along the axial direction. The LAMMPS package is adopted to conducted the NEMD simulations with a time step of 1 fs. The CNT and the graphene sheets are frozen to save the computational time. The Nosé-Hoover thermostat is used to control the temperature of system to 300 K, with a damping coefficient of 100 time steps. The time step is set as 1.0 fs. In our NEMD simulations, the system runs for 1.0 ns to reach a stable state, and then continues to run 4.0 ns to sample the simulation output. The sampling interval is 1.0 ps. In order to calculate the interfacial resistance, the flow of ion solutions with the same ion concentration in an interfacial CNT is also simulated.

2.2. Interfacial resistance

As the system is in a steady state, the external force driving fluid flow in the system is balanced by the internal resistance of CNT and the interfacial resistance of membrane. The internal resistance of CNT comes from the collision between molecules and CNT walls, and the interfacial resistance comes from the energy loss caused by molecules penetrating the liquid-solid interface. The flowrate passing the CNT membrane (J_{CNT}) can be computed following $J_{CNT} = A_{CNT}\rho_{CNT}v_{com}$. ρ_{CNT} is the ensemble averaged density of solutions in the CNT; v_{com} denotes the velocity of solution calculated by NEMD simulation and A_{CNT} is the cross-sectional area of CNT. The flowrate at the steady state can be obtained from the corrected diffusivity （D_o^{finite}）:

$$J_{CNT} = -A_{CNT}\rho_{CNT}\frac{D_o^{finite}}{k_B T}\frac{d\mu}{dz} \quad (1)$$

where $d\mu/dz$ is the chemical potential gradient and *T* represents the temperature. The corrected diffusivity can be calculated as:

$$D_o^{finite}(f) = \frac{k_B T J_{CNT}}{A_{CNT}\rho_{CNT}(f)\Gamma_{exe}} \quad (2)$$

where Γ_{exe} represents the external force determined from the chemical potential gradient over the CNT, following $\Gamma_{exe} = \mathrm{d}\mu/\mathrm{dz}$; One could understand that as long as the chemical potential difference between the feed and the permeate reservoirs is small, it is justified to approximate the external force Γ_{exe} following:

$$\Gamma_{exe} \equiv \frac{d\mu}{dz} = k_B T\frac{d\ln f}{dz} \cong k_B T\frac{f_1 - f_2}{fL_{CNT}} \quad (3)$$

Accordingly, combining the Eqs. (2) and (3), one can calculate the overall resistance comprising of the interfacial and intracrystalline resistances by

$$R_{tot} = \frac{\Delta f}{J_{CNT}} = \frac{f_1 - f_2}{J_{CNT}} = \frac{fL_{CNT}}{A_{CNT}\rho_{CNT}D_o^{finite}} \quad (4)$$

Following the same way, the internal resistance can be calculated by conducting NEMD simulations for the infinitely long CNT at the target pressure and temperature, written as

$$R_{internal} = \frac{f_1 - f_2}{J_{CNT}} = \frac{fL_{CNT}}{A_{CNT}\rho_{CNT}D_o^{infinite}} \quad (5)$$

where $D_o^{infinite}$ is the diffusivity in an infinite CNT. So, the interfacial resistance can be accordingly evaluated as,

$$R_{interf} = R_{tot} - R_{internal} = \frac{fL_{CNT}}{A_{CNT}\rho_{CNT}}\left(\frac{1}{D_o^{finite}} - \frac{1}{D_o^{infinite}}\right) \quad (6)$$

3. Results and discussion

The fluxes of water molecules in the ion solution with different ion concentrates flowing into CNT membranes for various CNT diameters are shown in the Figure.2(a). It can be seen from the figure that with the increase of ion concentration, the flux decreases. As the ion concentration increases from 0.5 M to 1.5 M, the flux reduces from 368.8 ns^{-1} to 310.0 ns^{-1} and the decline is

19.85 % for the case of (8,8) CNT. For (15,15) CNT, the flux decreases from 2136.7 ns^{-1} to 1800.3 ns^{-1} and the decline is 15.70%. By comparing the results of various dimeter, one term of conclusion can be obtained: the total resistance (interfacial resistance and internal resistance) for water molecules increases with the increase of ion concentration. The detailed total resistance values are shown in Figure. 2 (b).

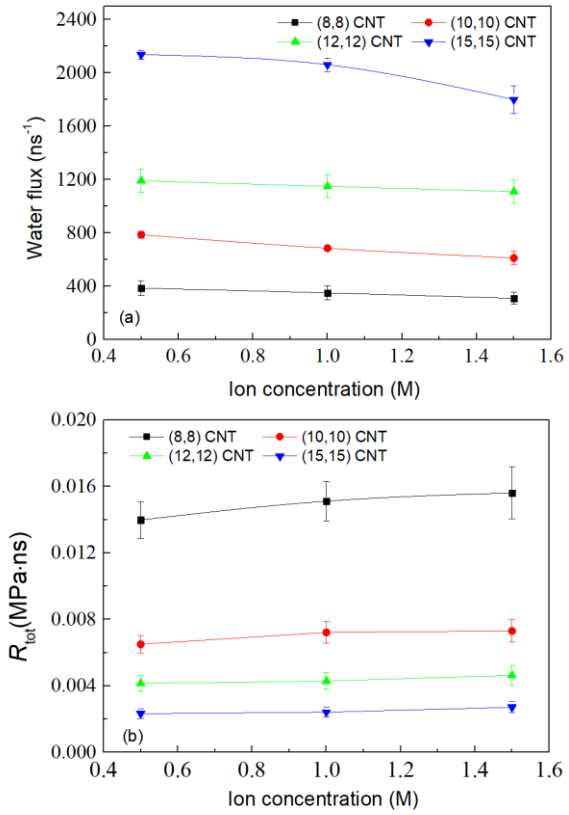

Fig. 2 (a) Function of the flux on the ion concentration, (b) Total resistance of water molecules with the ion concentration

Based on the relation of interface resistance and total resistance, $R_{interf} = R_{tot} - R_{internal}$, the interfacial resistance of water molecules with different ion concentrations and diameters of CNT are obtained and the results are illustrated in the Figure 2(b). The diameter of CNT increases with surface curvature, which weaken the resistance of CNT membrane to the solution, leading to the reduced interfacial resistance. Similar to the change of diameter, one can observe that with the increase of ion concentrations, the interfacial resistance increases. Compared with the values obtained for various diameters and same ion concentration, it can be found that the growth of interface resistance associated with larger diameter is faster than the smaller one. For example, the interfacial resistance increases by 55.20% in (8,8) CNT as the ion concentration rising from 0.5 M to 1.5 M, while only increases by 37.10% for (15,15) CNT.

The interfacial resistance and the ratio of interfacial resistance relative to the total resistance at different ion concentrations are shown in the Figure 3 (a) and (b). It is found that both the interfacial resistance and the ratio decrease with increase in the diameter of the CNT. The interfacial resistance accounts for more than 65% of the overall resistance, revealing the fact that the flow in the CNT membrane is determined by the interfacial resistance, which is agreement with previous works[18]. Although enhancing the ion concentration of system in the large diameter of CNT imposes fewer effect on the interfacial resistance, the ratio of interfacial resistance relative to the total resistance still increases due to the decline of total resistance.

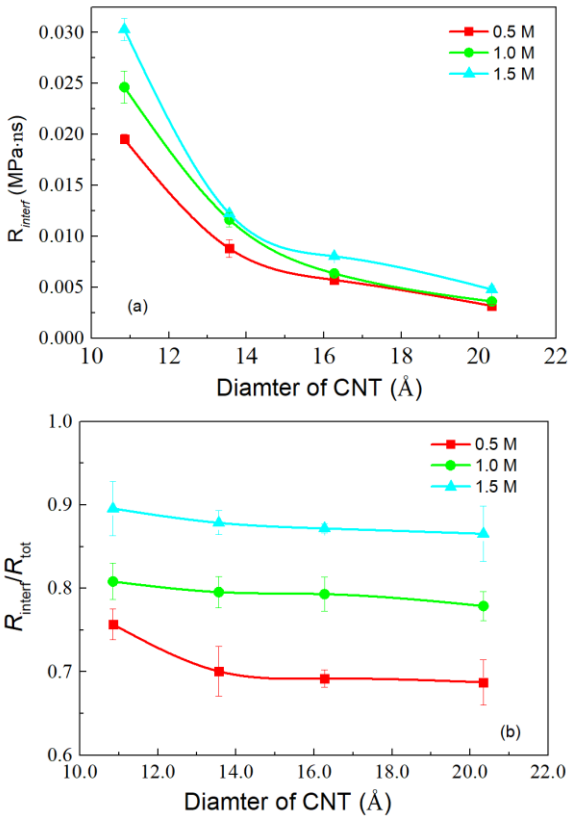

Fig.3 Dependencies of (a) interfacial resistance and of (b) fraction of interfacial resistance on the ion concentration

In our previous work[20], we found that the flow entering into the CNT membrane can be decompose into surface and direct flowrates, as shown in Figure 4. Therefore, the interface resistance is comprising of flange resistance and entrance-exit resistance. The flange resistance arises from the streamline bending effect of fluid molecules adsorbed on the graphene sheets and the entrance-exit resistance attributed to the thermodynamic resistance for fluid molecules traversing the interfacial phase to enter the confining CNT from the

free bulk phase. According to this conclusion, the influence of ion concentration and CNT diameter on the interface resistance will be analyzed from entrance-exit resistance and flange resistance.

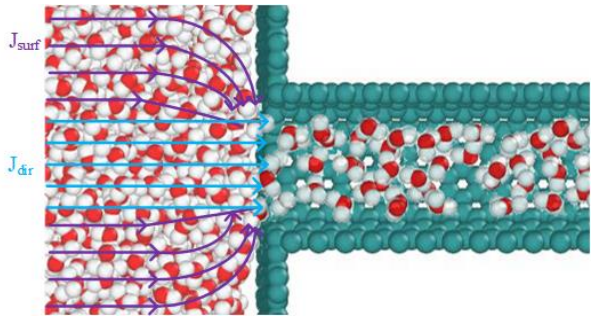

Fig. 4 Definitions of surface and direct flowrates

In order to explain the entrance-exit resistance when the water flows into the CNT membrane, the potential mean force (PMF) of water molecules is calculated and the results are shown in the Figure 5. In the figure, 0.0 represents the entrance position of CNT membrane. The PMF [23]was determined as the difference between the excess chemical potentials of water at the local position z, μ_z^{ex}, and in the bulk reservoir, μ_{bulk}^{ex}, as:

$$\mu_z^{ex} - \mu_{bulk}^{ex} = -k_B T \ln(\rho_z / \rho_{bulk}) \quad (7)$$

where k_B is Boltzmann constant, ρ_z and ρ_{bulk} are the number density of water at position Z and in bulk reservoir, respectively. The fluctuation in the case of (8,8) CNT is caused by the highly ordered structure of water molecules in CNT. The same fluctuation was also observed in the study of Liu et al[24]. It can be seen from the figures that the differences between valley and peak of PMF increase with the decrease of CNT diameter and increase of ion concentration. From Figure 5(a), the diameter of CNT decreases from 1.085 nm to 2.034 nm, and the corresponding energy barrier reduces from 3.37 KJ/mol to 2.03 KJ/mol. The reduction energy barrier with diameters and ion concentrations indicates the decrease of entrance-exit resistance.

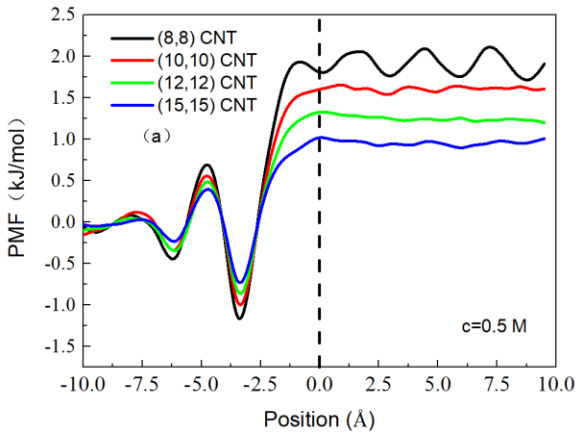

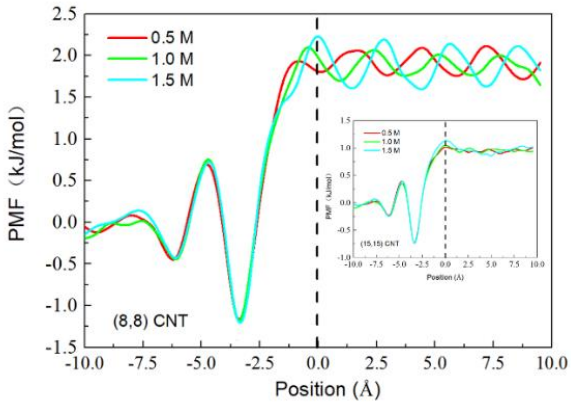

Fig.5 (a) PMF of water for CNT at different diameters at 0.5 M, (b) PMF of water in the (8,8) CNT for different ion concentrations, the inset for the case of (15,15) CNT

The flange resistance is another important component of interfacial resistance coming from the streamline bending effect of graphene sheet. So, the density profiles of water molecules near the graphene sheet are calculated to explain the influence of CNT diameter and ion concentrations on the flange resistance and the results are shown in the Figure 6. It can be seen from the Figure 6(a) that the density of water molecules is close to be the bulk one in the region away from the CNT membrane, indicating that the water molecules are not be affected. Figure 6(b) reveals that the peak density of water decreases when the diameter of CNT being enlarged. As a consequence of that, the proportion of water molecules subjected to the streamline bending effect are anticipated to be reduced, which accounts for the decreased flange resistance in the larger CNTs. In resemblance to the change of flange resistance for various diameters of CNT, one can find that the density of water with decrease of ion concentrations has the similar change as shown in the Figure 6(b).

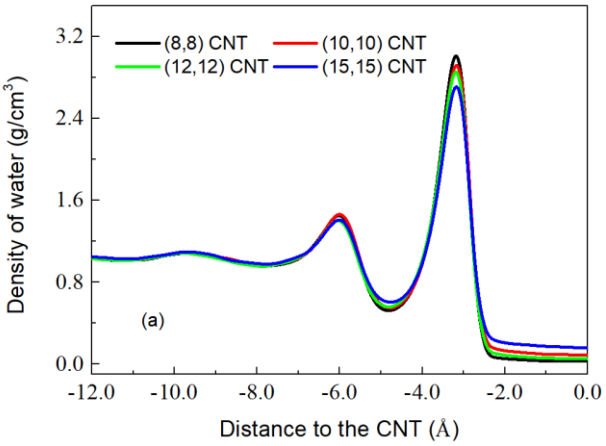

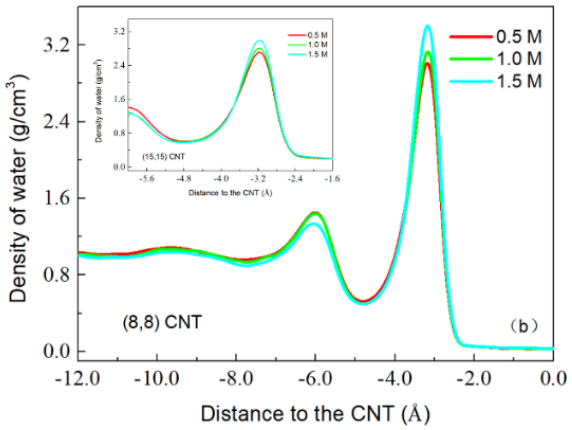

Fig.6 (a) Density of water at the entrance region for various diameters of CNTs, (b) Density of water in the (8,8) CNT membrane at the entrance region for various ion concentrations, the inset for the case of (15,15) CNT

In summary, both the entrance-exit resistance and flange resistance enhance with the decrease of CNT diameter and the increase of ion concentration, resulting in the change of interfacial resistance as shown in Figure. 2. The reason for this is the presence of cations (Mg^{2+} and Li^{+}) in the solution, and the detailed ions profiles are described below.

In order to explain how the cations affect the interfacial resistance of water molecules, the distribution of the number of cations in the system is calculated, and the results are shown in Figure. 7. One can find that as the increase of ion concentration, the color of the area near the entrance of CNT membrane displays deepened, indicating that the number of ions in this area gradually increased. The increase of ions will lead to a tighter water substructure and an increase in the local density of water molecules. And, the aggregation of ions in the entrance region of CNT will hinder the entrance of water molecules into CNT membrane and increase the energy barrier for water molecules. By comparing the results of different CNT diameters, it can be seen from the figure that the number of ions for the smaller CNT is larger than the bigger one at the same ion concentration, that is, the influence of ion concentration on transport decreases with the increase of CNT diameter. The reason for this is that the energy barrier of Mg^{2+} and Li^{+} entering CNT decreases with the increase of CNT diameter[16].

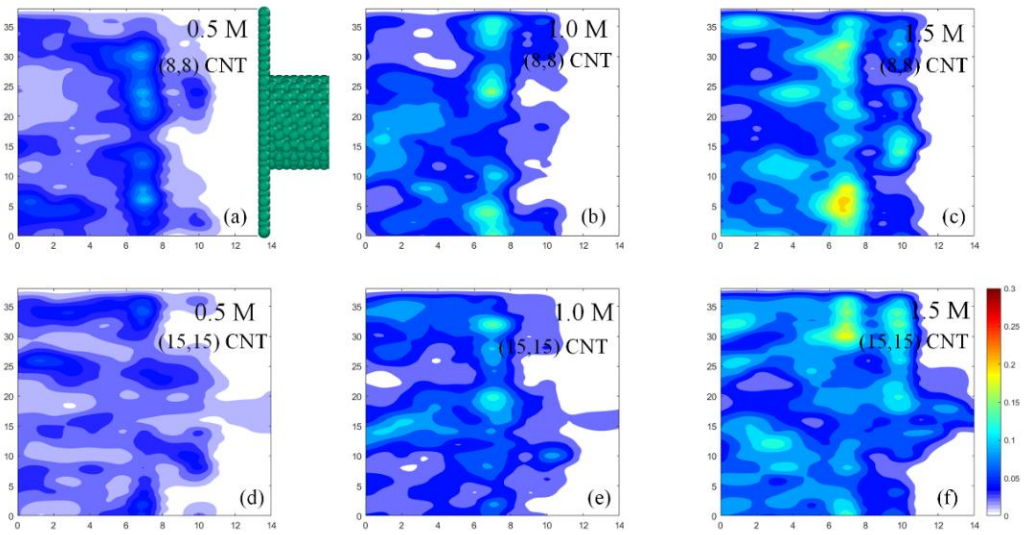

Fig.7 Profile of number of cations in the entrance region of CNT membrane

4. CONCLUSIONS

We have conducted a systematic study on the transport flow of ion solution composed of LiCl/MgCl2 in the CNT membranes with different pore sizes ranging from 0.81 to 2.034 nm, at 300 K. The interfacial resistance dominates the mass transport resistance in the CNT membrane and the proportion increases with the increase of ion concentration and diameter of CNT. We decompose the interfacial resistance into two components including the flange-resistance and the entrance-exit resistance to explain the effect of ions concentration and diameter on the interfacial resistance. It is found when increases the ion concentration of system, both the entrance-exit resistance and flange resistivity decrease, consequently leading to the reduced interfacial resistance, associated with enhanced flow crossing the CNT membranes. To a large extent, this change is due to aggregation of ions in the entrance of CNT membrane with increase of the energy barrier for ions.

ACKNOWLEDGEMENT

L. Liu acknowledges National Natural Science Foundation of China [Grant No. 52006017] for the

funding support and China Postdoctoral Science Foundation for funding support (2021M690175). Thanks the financial support of the Frontier Crossover Project of Central Universities (2021CDJQY-029).

REFERENCE

[1] I.G. Wenten, P.T. Dharmawijaya, P.T.P. Aryanti, R.R. Mukti, K. Khoiruddin, LTA zeolite membranes: current progress and challenges in pervaporation, RSC Advances 7(47) (2017) 29520-29539.
[2] X. Wang, J.Z. Sun, B.Z. Tang, Poly(disubstituted acetylene)s: Advances in polymer preparation and materials application, Progress in Polymer Science 79 (2018) 98-120.
[3] L. Wang, S. Lin, Mechanism of Selective Ion Removal in Membrane Capacitive Deionization for Water Softening, Environ Sci Technol 53(10) (2019) 5797-5804.
[4] T. Luo, S. Abdu, M. Wessling, Selectivity of ion exchange membranes: A review, Journal of Membrane Science 555 (2018) 429-454.
[5] F.M. Gunawan, D. Mangindaan, K. Khoiruddin, I.G. Wenten, Nanofiltration membrane cross-linked by m -phenylenediamine for dye removal from textile wastewater, Polymers for Advanced Technologies 30(2) (2019) 360-367.
[6] Y. Zhao, Z. Zhong, Z.-X. Low, Z. Yao, A multifunctional multi-walled carbon nanotubes/ceramic membrane composite filter for air purification, RSC Advances 5(112) (2015) 91951-91959.
[7] P. Xu, J. Hong, Z.Z. Xu, H. Xia；, Q.-Q. Ni；, Positively charged nanofiltration membrane based on (MWCNTs-COOK)-engineered substrate for fast and efficient lithium extraction, Separation and Purification Technology 270(1) (2021) 118796.
[8] S.Y. Sun, L.J. Cai, X.Y. Nie, X. Song, J.-G. Yu, Separation of magnesium and lithium from brine using a nanofiltration membrane, Journal of Water Process Engineering 7 (2015) 210-217.
[9] Z. Zakaria, S.K. Kamarudin, S.N. Timmiati, Membranes for direct ethanol fuel cells: An overview, Applied Energy 163 (2016) 334-342.
[10] S. Ali, S.A.U. Rehman, H.Y. Luan, M.U. Farid, H. Huang, Challenges and opportunities in functional carbon nanotubes for membrane-based water treatment and desalination, Science of the Total Environment 646 (2019) 1126-1139.
[11] Ihsanullah, Carbon nanotube membranes for water purification: Developments, challenges, and prospects for the future, Separation and Purification Technology 209 (2019) 307-337.
[12] L. Liu, D. Nicholson, S.K. Bhatia, Effects of Flange Adsorption Affinity and Membrane Porosity on Interfacial Resistance in Carbon Nanotube Membranes, ACS Appl Mater Interfaces 10(40) (2018) 34706-34717.
[13] L. Liu, D. Nicholson, S.K. Bhatia, Exceptionally high performance of charged carbon nanotube arrays for CO2 separation from flue gas, Carbon 125 (2017) 245-257.
[14] L. Liu, C. Hu, D. Nicholson, S.K. Bhatia, Inhibitory Effect of Adsorbed Water on the Transport of Methane in Carbon Nanotubes, Langmuir 33(25) (2017) 6280-6291.
[15] B. Corry, Designing carbon nanotube membranes for efficient water desalination, Journal of Physical Chemistry B 112(5) (2008) 1427-1434.
[16] D.F. Yang, Q.Z. Liu, H.M. Li, C. Gao, J., Molecular simulation of carbon nanotube membrane for Li+ and Mg2+ separation, Journal of Membrane Science 444 (2013) 327-331.
[17] M.E. Suk, A.V. Raghunathan, N.R. Aluru, Fast reverse osmosis using boron nitride and carbon nanotubes, Applied Physics Letters 92 (2008) 133120.
[18] L. Liu, D. Nicholson, S.K. Bhatia, Interfacial resistance and length-dependent transport diffusivities in carbon nanotubes, The Journal of Physical Chemistry C 120(46) (2016) 26363-26373.
[19] X. Zhang, W. Zhou, F. Xu, M. Wei, Y. Wang, Resistance of water transport in carbon nanotube membranes, Nanoscale 10(27) (2018) 13242-13249.
[20] Q. Wang, L. Liu, L. Han, C. Liu, Y. Liu, Exchange dynamics of molecules at the fluid-solid interface determining the diffusion rate in nanopores, Journal of Molecular Liquids 335 (2021) 116030.
[21] Y. Zhu, Y. Ruan, Y. Zhang, Y. Chen, X. Lu, L. Lu, Mg2+-Channel-Inspired Nanopores for Mg2+/Li+ Separation: The Effect of Coordination on the Ionic Hydration Microstructures, Langmuir : the ACS journal of surfaces and colloids 33(36) (2017) 9201-9210.
[22] Q. Wang, L. Liu, C. Liu, J. Song, X. Gao, Size effect in determining the water diffusion rate in carbon nanotubes, Journal of Molecular Liquids 334 (2021).
[23] L. Liu, D. Nicholson, S.K. Bhatia, Effects of flange adsorption affinity and membrane porosity on interfacial resistance in carbon nanotube membranes, ACS applied materials & interfaces 10(40) (2018) 34706-34717.
[24] L. Liu, G.N. Patey, Simulated conduction rates of water through a (6,6) carbon nanotube strongly depend on bulk properties of the model employed, The Journal of chemical physics 144(18) (2016) 184502.